Fluorogenic Substrates and Cyclic Peptide Inhibitors of the Oligonucleotide Activated SIRT7

Julie E. Bolding,[1] Alexander L. Nielsen,[1,4] Iben Jensen,[1] Line A. Ryberg,[2] Samuel T. Jameson,[1] Pernille Harris,[2,5] Günther H. J. Peters,[2] John M. Denu,[3] Joseph M. Rogers,[1,*] and Christian A. Olsen[1,*]

[1]*Center for Biopharmaceuticals & Department of Drug Design and Pharmacology, Faculty of Health and Medical Sciences, University of Copenhagen, DK-2100, Copenhagen, Denmark.*

[2]*Department of Chemistry, Technical University of Denmark, Kgs. Lyngby, DK-2800, Denmark.*

[3]*Department of Biomolecular Chemistry, University of Wisconsin-Madison, Madison, Wisconsin 53706, United States & Wisconsin Institute for Discovery, University of Wisconsin-Madison, Madison, Wisconsin 53715, United States*

[4]*Present address: Institute of Chemical Sciences and Engineering, École Polytechnique Fédérale de Lausanne (EPFL), CH-1015, Lausanne, Switzerland.*

[5]*Present address: Department of Chemistry, University of Copenhagen, DK-2200, Copenhagen, Denmark.*

**Correspondence: joseph.rogers@sund.ku.dk (J.M.R), cao@sund.ku.dk (C.A.O.)*

Abstract

The sirtuins are NAD^+-dependent lysine deacylases, comprising seven isoforms (SIRT1–7) in humans, which are involved in the regulation of a plethora of biology, including gene expression and metabolism. The sirtuins share a common hydrolytic mechanism but display preferences for different ε-*N*-acyllysine substrates. SIRT7 deacetylates targets in nuclei and nucleoli but remains one of the lesser studied of the seven isoforms; in part, because of a lack of chemical tools to specifically probe SIRT7 activity. Here we expressed SIRT7 and, using small-angle X-ray scattering, reveal SIRT7 to be a monomeric enzyme with low degree of globular flexibility in solution. We developed a fluorogenic assay for investigation of the substrate preferences of SIRT7 and to evaluate compounds that modulate its activity. We report several mechanism-based SIRT7 inhibitors and *de novo* cyclic peptide inhibitors selected from mRNA-display library screening; compounds that represent starting points for development of the needed SIRT7-specific chemical tools.

Keywords**:** S*irtuins, SIRT7, posttranslational modification, fluorescence assay, nucleosomes, SAXS, cyclic peptides, mRNA display, RaPID system, SIRT inhibitors*

Introduction

The sirtuins are a group of NAD^+-dependent lysine deacylase enzymes with seven isoforms (SIRT1–7) present in humans. The enzymes share a conserved catalytic site and nucleotide binding pocket but serve distinct cellular roles and have different substrate preference and subcellular localization.[1] The biological roles of SIRT7 remain less well established than for other sirtuin isoforms. SIRT7 is predominantly localized to the nucleus and centers around the nucleoli where it interacts with RNA polymerases and histone proteins.[2] It has been found to remove acetyl,[3] propionyl,[3b] glutaryl,[4] and succinyl[5] posttranslational modifications from the ε-amino groups of lysine residues in a variety of proteins. The acetylated histone 3 lysine 18 (H3K18ac) and lysine 36 (H3K36ac) are among the most studied targets, being involved in a range of regulatory roles.[3a, 6]

For example, SIRT7 has been found to play a role in DNA repair,[5, 6c] rDNA stability and pre-rRNA processing,[2a, 7] endoplasmic reticulum stress,[8] mitochondrial homeostasis,[9] energy metabolism,[10] and bone formation.[3b] SIRT7 has also been implicated in different diseases,[6e, 11] including tumorigenesis.[12] Despite its main documented role as a deacetylase, SIRT7 more efficiently catalyzes the removal of ε-*N*-acyllysine modifications of longer length in biochemical assays *in vitro* [6f, 13] and has been shown to exert improved catalytic efficiency in the presence of various oligonucleotide additives [13a, 14] or reconstituted nucleosome particles.[6f, 13b, 14] It is well documented that the catalytic activity of both SIRT1 and SIRT6 can be enhanced by allosteric binders[15] and the activity of SIRT6 is increased by binding to nucleosomes[16] with high affinity through its intrinsically disordered C-terminus.[17] SIRT7, on the other hand, has extended N- and C-termini that are positively charged and have been proposed to interact with negatively charged patches of oligonucleotides.[14] Structural elucidation of SIRT7 is challenging and has thus far been limited to computational predictions[18] and an X-ray crystal structure of a fusion protein containing the N-terminal domain of SIRT7.[19] Despite the intriguing biological implications of SIRT7, the development of modulators of its activity has been limited.[20]

Here, we establish a protocol for expression of catalytically active SIRT7 enzyme that is amenable to storage and small angle X-ray scattering (SAXS) show that SIRT7 is monomeric in solution and has a low degree of overall flexibility. With this enzyme in hand, we have developed an assay, which allows for semi-high-throughput evaluation of activators and inhibitors of the SIRT7 activity. Using this assay, several SIRT7 inhibitors were designed and, finally, *de novo* screening of large libraries of peptides, led to the discovery of a novel potent cyclic peptide inhibitor.

Results and discussion

Because the SIRT7 obtained from commercial sources generally lack hydrolytic activity, it has been challenging to develop broadly applicable and efficient screening assays for determining substrate specificity of the enzyme and develop modulators of its activity. One previous assay was developed by Lin and co-workers, using recombinant His-tagged SIRT7 and HPLC-based evaluation of the SIRT7-mediated hydrolysis of PTMs from histone peptides of 12- to 15-mer length.[13a, 14] However, we were interested in improving the throughput of the

assay to enable more systematic evaluation of substrates and modulators of SIRT7. Also, because the N- and C-termini of the enzyme have been proposed to be involved in oligonucleotide recognition and be of importance for catalysis, we designed a construct in which the affinity tag could be removed by introducing a tobacco etch virus (TEV) protease cleavage site. We envisioned that SAXS could provide biophysical characterization and lower resolution structural insight into wildtype SIRT7.

Thus, samples of purified SIRT7 ranging from a concentration of 1.02 mg/mL to 3.91 mg/mL were prepared and subjected to SAXS measurement. From visual inspection of the resulting SAXS curves, the overall shapes of the curves did not change with increasing concentration and molecular masses derived from the SAXS data ranged from 40–46 kDa corresponding to a single SIRT7 monomer (45 kDa) (Supporting Figure S1). Further, a Kratky plot indicated that the protein is folded with low flexibility (Supporting Figure S1). A merged curve was generated from the data recorded at low and high concentration and this curve was used for modeling. A structure of human SIRT7 has been predicted using the AlphaFold2 structure prediction (PDB Q9NRC8) (Figure 1).[18b, 21] Overall, the model confidence is high or very high for the N-terminal domain and the Rossman fold containing catalytic domain. For the N-terminal domain this likely reflects that an X-ray crystal structure is available (residues 5–73; PDB 5IQZ)[19] and for the Rossman fold domain there is high sequence similarity to SIRT6, for which several structures are available (*e.g.,* PDB 3K35,[22] 6XV1,[23] 7CL0,[24] 8F86,[16b] 8G57[16c])

AlphaFold2 confidently predicts the N-terminus to be three a-helices that are very solvent-exposed. AlphaFold2 also predicts the inter-domain accuracy between these helices and the Rossman fold; it has confidence in orientation of N-terminus and how it projects from the catalytic domain. In contrast, the model confidence is either low or very low for the C-terminal domain from residues 364–400. The theoretical scattering curve for the AlphaFold2 model shows a reasonable fit to the merged experimental scattering curve with $c^2 = 2.3$ (Figure 1B) and superimpose well with the generated SAXS envelope (Figure 1C). To improve the fit, modeling with Coral was carried out allowing flexibility in the C-terminal residues 365–371 for which the model confidence is very low in the AlphaFold2 prediction. The resulting Coral model has an improved fit to the experimental scattering curve with $c^2 = 1.3$ (Figure 1B) and superimpose well with the SAXS envelope (Figure 1D). The Coral model has a different conformation of the C-terminus compared to the AlphaFold2 model, suggesting that the C-terminus does not bind to the Rossman fold (Figure 1C,D), which is in line with the low/very low confidence in the AlphaFold2 model in this area (Figure 1A). Taken together, our data fitting may reflect some degree of flexibility of the C-terminal domain, which is not seen in the generated Kratky plot; likely, because the C-terminal domain is a minor fraction of the protein. Whether the C-terminus may interact with substrate as well as the Rossman domain to bring the substrate into proximity with the active site will require high-resolution structural insight.

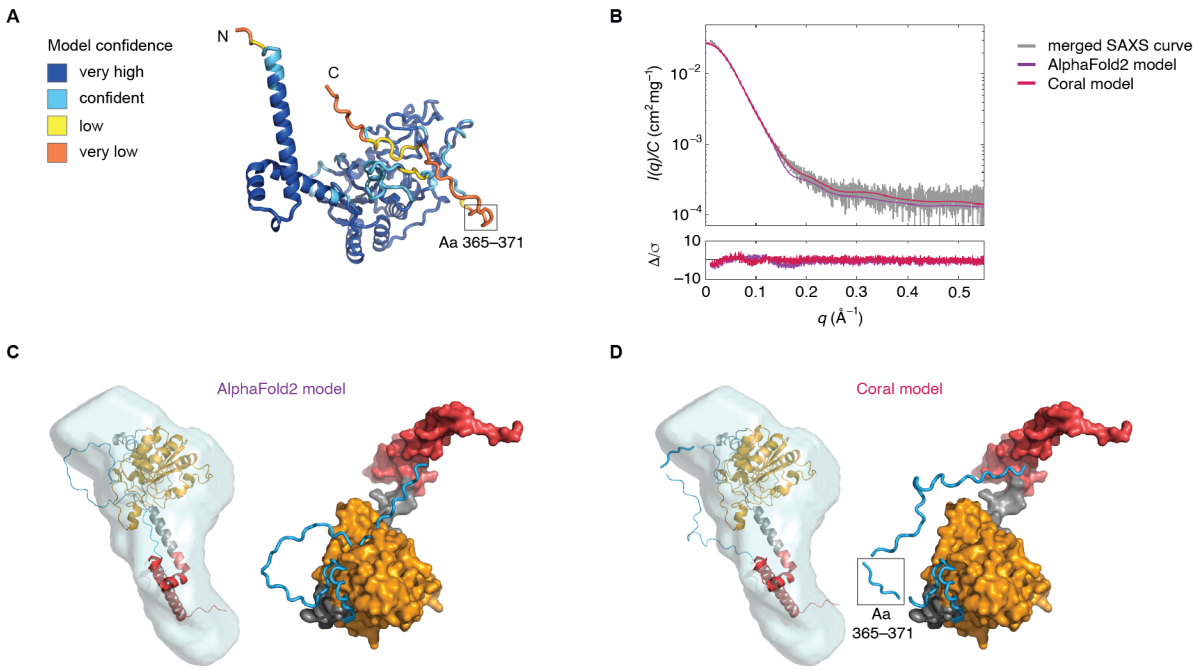

Figure 1. Small angle X-ray scattering. (**A**) The AlphaFold2 model of human SIRT7 colored by model confidence based on the per-residue confidence score (pLDDT): very high (pLDDT > 90), confident (pLDDT = 90–70), low (pLDDT = 70–50), and very low (pLDDT < 50). Residues 365–371 (black box) were flexible in the Coral modeling. (**B**) Crysol fits of the AlphaFold2 and the Coral model to the experimental SAXS data. (**C,D**) Superposition of the SAXS derived envelope with the Alphafold2 model and the Coral model, respectively. Structural representation of the model with N-terminus (red) and Rossman fold and catalytic domain (orange) shown as surface view and the C-terminus (blue) shown as cartoon.

Past efforts in our laboratory have included screening of the activities of sirtuin and HDAC enzymes to determine their substrate preferences,[25] primarily by applying trypsin-coupled assays with the release of a C-terminal-conjugated 7-amino-4-methylcoumarin (AMC) fluorophore.[26] We therefore performed a screening of the activity of our recombinant SIRT7 against a library of 40 selected fluorogenic substrates, based on five different peptide sequences. We further included oligonucleotide additives previously reported by Lin and co-workers to enhance the catalytic efficacy of SIRT7, i.e., double-stranded DNA (salmon sperm DNA sheared to an average size of less than 2000 base pairs) or yeast tRNA (Figure 2A,B).[13a, 14] Generally, we observed a significantly lower activity of SIRT7 compared to the activity observed for other isoforms (SIRT1–3 and SIRT5) against their preferred substrates. We found that SIRT7 displays low activity against our selection of acetylated (Kac) fluorogenic substrates, despite acetylation being the most reported posttranslational modification hydrolyzed by SIRT7.[27] We observed the highest activity of recombinant SIRT7 against hexanoyl (Khex, C_6), octanoyl (Koct, C_8), decanoyl (Kdec, C_{10}) and lauryl (Klau, C_{12}) containing substrates. Substantially higher conversions were observed for the substrates based on the QPKKacyl and TARKacyl peptide sequences compared to the alternative three peptide sequences with the same acyl group, suggesting an increased activity against substrates containing a positively charged amino acid residue in the *i*-1 position. Interestingly, the two reported SIRT7 targets H3K18ac and H3K36ac both have neighboring positively charged amino acid residues. In agreement with previously reported observations,[13a, 14] we found that hydrolytic activity was enhanced substantially in the presence of the

oligonucleotides and particularly by the addition of tRNA. While the maximum degree of hydrolysis was observed for the Ac-QPKKlau-AMC substrate, we found that its low aqueous solubility was prohibitive at the desired substrate concentration (50 µM final concentration). Thus, we proceeded with the assay development using Ac-QPKKdec-AMC, for which the second highest degree of hydrolysis was obtained. First, a titration of SIRT7 was performed in the presence or absence of oligonucleotides, which showed a linear correlation between substrate conversion and SIRT7 concentration (Figure 2C). Next, we performed a titration of DNA and tRNA activation with Ac-QPKKdec-AMC and observed a normal distribution relationship between oligonucleotide concentration and deacylation activity, with a maximum activation of 800% in the presence of SIRT7–tRNA (1:8 mol/mol). A further increase in tRNA concentration resulted in a Hook effect, where activity decreased (Figure 2D).

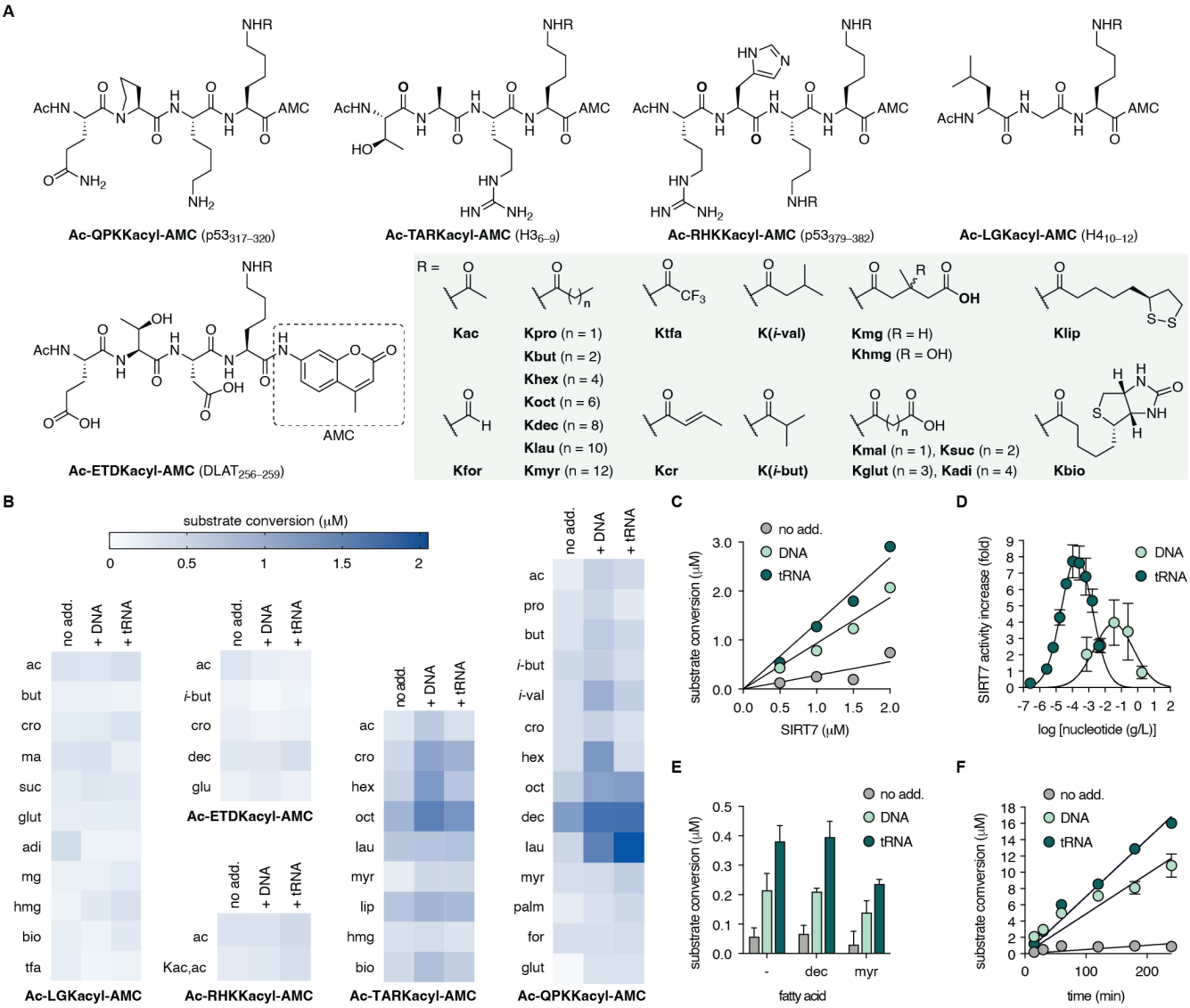

Figure 2. Screening for substrates of SIRT7. (**A**) Substrate sequences and acyl groups (for novel substrates, see Supporting Figure S2). (**B**) Heatmap of SIRT7-dependent deacylase activity [1 h incubation at 37 °C with SIRT7 (500 nM), substrate (50 µM), NAD^+ (500 µM), and DNA (75 µg/mL) or tRNA (37 µg/mL)]. For data values, see Supporting Table S1. (**C**) Titration of SIRT7 using Ac-QPKKdec-AMC (50 µM) as substrate. (**D**) Titration of DNA and tRNA using Ac-QPKKdec-AMC (50 µM) as substrate. (**E**) Activation of SIRT7-dependent deacetylation of substrate Ac-QPKKac-AMC (50 µM) by

fatty acids. (**F**) SIRT7-mediated hydrolysis over time, using Ac-QPKKdec-AMC (50 μM) as substrate. All data are based on two individual experiments performed in duplicate. Error bars represent the mean ± SD.

Both SIRT6 and SIRT7 belong to the class IV gene family and because SIRT7 mainly acts as a deacetylase in cells, while displaying a preference for long-chain acyl modifications in our fluorogenic assays, we envisioned that SIRT7 deacetylation could be activated by the presence of fatty acids as observed for SIRT6 [15a]. However, no increase in catalytic activity of SIRT7 was observed in the presence of neither capric- nor myristic acid (Figure 2E). Lastly, we tested the assay linearity over time; given the lower catalytic activity of recombinant SIRT7 compared to the catalytic efficiency of SIRT1–3 and SIRT5 in fluorogenic assays.[25a, 25c, 28] The assay progression, and the SIRT7 stability (in presence of either DNA or tRNA), remained linear for up to 4 h at 37 °C (Figure 2F).

After observing that SIRT7 exhibited preference for the Ac-QPKKacyl-AMC substrates, which is based on the $p53_{317\text{-}320}$ amino acid sequence, we envisioned that catalysis could be further enhanced by designing a substrate mimicking the sequences of well documented histone target sites. Past reports from Lin and co-workers monitored SIRT7 deacylation using an H3K9 sequence, instead of the validated SIRT7 targets on histone 3, which were H3K18 and H3K36[3a, 6] and more recently also H3K37.[6f] We therefore synthesized the fluorogenic $H3_{15–18}$ (Ac-APRKacyl-AMC) and $H3_{33–36}$ (Ac-GGVKacyl-AMC) substrates (Figure 3A) and monitored the SIRT7-mediated hydrolysis of these in presence of tRNA. Given the resemblance of the QPKK and the APRK sequence, it was not surprising that the catalytic efficiency towards the two were in the same range. Nevertheless, we observed a slight increase in in activity of approximately 2-fold when applying the Ac-APRKacyl-AMC substrate. The GGVK motif, on the other hand, gave substantially lower conversion, which we speculate might be due to the lack of the positive charge from the K37 residue in the natural substrate. Again, we observed substantially lower deacetylase and demyristoylase activity compared to dedecanoylase activity (Figure 3B). We next attempted to perform kinetic experiments to determine Michaelis-Menten parameters with tRNA as an additive but, unfortunately, the data did not allow fitting to the equation due to an estimated K_M of >100 μM (Supporting Figure S3). Because nucleosomes have also been shown to activate SIRT7,[13b] we instead turned to reconstituted nucleosome particles as an additive. Using the best performing substrate from the tRNA-activated tests (Figure 3B), we performed a titration of the concentration of nucleosomes added, showing optimal substrate conversion at 250 nM with a SIRT7 concentration of 500 nM (Figure 3C). The level of conversion of substrate **1b** under nucleosome activation enabled determination of Michaelis-Menten parameters, giving a K_M of 12 μM (Figure 3D), which is somewhat higher than determined for longer histone peptides.[13b]

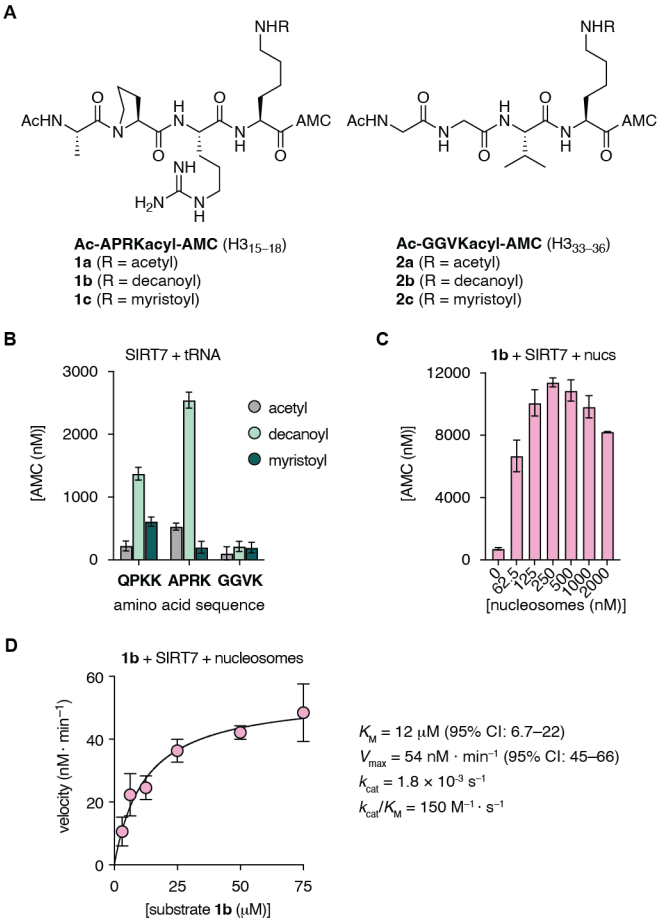

Figure 3. Novel substrates, activation by nucleosomes, and Michaelis-Menten kinetics for SIRT7. (**A**) Structures of fluorogenic substrates based on the sequence of known target sites of SIRT7 in histone 3 (**1a**–**c** and **2a**–**c**). For chemical synthesis, see Supporting Figure S2. (**B**) SIRT7-mediated hydrolysis of selected substrates. Conditions: SIRT7 (500 nM), substrate (50 μM), NAD^+ (500 μM), tRNA (4 μM). All reactions were incubated for 1 h at 37 °C. (**C**) SIRT7-mediated hydrolysis of substrate **1b** in the presence of nucleosomes. Conditions: SIRT7 (500 nM), substrate (50 μM), NAD^+ (500 μM), nucleosomes (62.5–2000 nM). All reactions were incubated for 1 h at 37 °C. (**D**) Michaelis-Menten kinetics for SIRT7-mediated hydrolysis of substrate **1b** in the presence of nucleosomes. Conditions: SIRT7 (500 nM), substrate (3.125–75 μM), NAD^+ (500 μM), nucleosomes (200 nM). All reactions were incubated for 1 h at 37 °C.

With our assay protocol established, we performed a structure–activity relationship (SAR) study to develop a potent inhibitor of SIRT7 as previously achieved for SIRT2, 3, and 5.[29] First, we tested a selection of known sirtuin inhibitors with varying selectivity profiles, including nicotinamide,[30] **EX-527**,[31] **TM**,[32] a macrocyclic peptide **S2iL5**,[33] and three thiourea-containing mechanism-based inhibitors developed in our own lab [25f, 29a, 29b] (Supporting Figure S4). Compound **3** was the most potent inhibitor of the dedecanoylase activity of SIRT7 by a modest 26% at 100 μM inhibitor concentration (Figure 4A), and we therefore used its scaffold as the starting point for further improvement. We first tested a selection of ε-*N*-acyllysine mimics (**4**–**7** Figure 4B), including a Ksuc mimic due to the reported desuccinylase activity of SIRT7,[5] but none of these compounds, including the inverse thioamide (**7**), exhibited substantially improved potency. Next, we attempted to improve potency by substituting the amino acids in the *i*+2 position (Figure 4C) and *i*+1 position (Figure 4D), respectively. Compounds **8**–**13**

revealed that an increase in potency could be achieved with a negatively charged side chain in the *i*+2 position and D-glutamate (**11**) even provided inhibition at 10 μM compound concentration (Figure 4C). The importance of the residue in the *i*+1 position was investigated by synthesizing compounds **14**–**29**, encompassing variations in both size, polarity, and stereochemistry (Figure 4D). Most substitutions caused a decrease in potency with positively charged side chains (**20**–**22**) being very poorly tolerated and the introduction of D-amino acids (**21** and **24**) leading to a decrease in potency as well. Negatively charged and hydrophobic residues were better accommodated and compound **27**, containing and L-valine residue, was the most potent of the series.

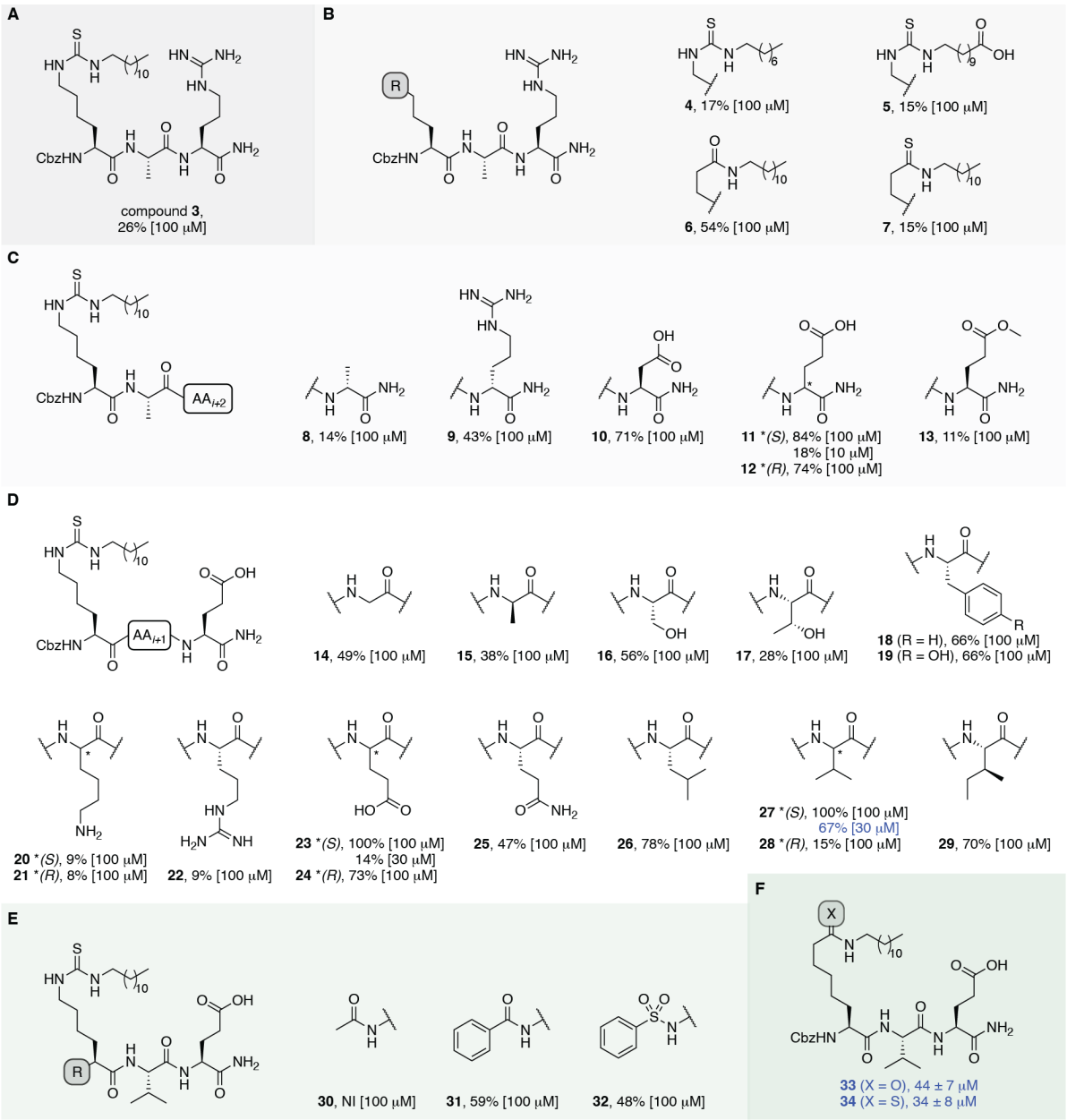

Figure 4. Structure-activity relationship study of SIRT7 inhibitors. (**A**) Lead compound **3**.[29b] (**B**) Amide isosteres. For chemical synthesis, see Supporting Figure S5. (**C**) Optimization of the *i*+2 position. For chemical synthesis, see Supporting Figure S5. (**D**) Optimization of the *i*+1 position. For chemical synthesis, see Supporting Figure S5. (**E**) N-terminal derivatization. For chemical synthesis, see Supporting Figure S5. (**F**) Final inverse (thio)amide inhibitors. For chemical synthesis, see Supporting Figure S5. Potencies are given as mean IC_{50}-values ± SD or %-inhibition at denoted concentrations,

using recombinant SIRT7 (500 nM), tRNA (4 μM), NAD^+ (500 μM), and Ac-QPKKdec-AMC (50 μM). Data are based on two individual experiments performed in duplicate.

We then briefly investigated the importance of the N-terminal group by synthesizing the acetyl, benzamide, and phenylsulfonamide analogues (**30**–**32**; Figure 4E), which all led to a significant loss in potency. Finally, we therefore synthesized inverse amide (**33**) and inverse thioamide (**34**) analogues based on the scaffold of the most potent thiourea-containing compound (**27**) in the SAR study (Figure 4F). Unfortunately, the most potent inhibitors (**33** and **34**), exhibited potencies in the micromolar range (34–44 μM), which is substantially higher than previously achieved with mechanism-based chemotypes against other SIRT isoforms.

We therefore used the "RaPID" screening platform, which has successfully furnished high-affinity cyclic peptides for a range of targets,[34] including SIRT2,[33] where binding was aided by a SIRT-targeting mechanism-based warhead. RaPID uses the ribosome to synthesize and screen large numbers ($>10^{12}$) of peptides containing non-canonical amino acids that allow for cyclization. Here, the first amino acid of each peptide was reprogrammed to the non-canonical *N*-chloroacetyl-D-phenylalanine, which reacts spontaneously with a cysteine residue to form stable, thioether-containing macrocyclic structures. An mRNA library was constructed, encoding peptides starting with the *N*-chloroacetyl-D-phenylalanine, followed by 4–12 randomized canonical amino acids and then a cysteine (Figure 5A). We chose to omit a mechanism-based warhead, which could contribute to binding to other sirtuins, relying instead on just the peptide structure for specific interactions with SIRT7. mRNA display was then used to covalently attach each cyclic peptide, after synthesis by the ribosome, to its encoding mRNA. This mRNA was reverse transcribed to generate the complimentary DNA that, after screening, could be sequenced to identify the SIRT7-binding cyclic peptides. We first incubated our RaPID library with immobilized full-length SIRT7. However, it became clear that SIRT7 was binding the oligonucleotide tag rather than the peptides (Supporting Figure S6A), consistent with the activation of SIRT7 by oligonucleotides (*vide supra*) that presumably bind to the enzyme. To allow selection based on peptide interaction with SIRT7, we followed two strategies. First, we added random DNA and RNA to outcompete any interaction between the full-length SIRT7 and the oligonucleotide tag. Second, we designed an additional SIRT7 construct that retained the enzymatic core but lacked the regions believed to drive nucleic acid binding, namely the N- and C-termini.[35] We removed the N-terminal–lysine and arginine-rich–helical region, which projects from the core domain in the AlphaFold2 prediction. We also removed the C-terminal region that has low AlphaFold2 confidence score (pLDDT) and is likely to be disordered, leaving the core enzymatic domain amino acids 74–363 (Figure 5B). A RaPID selection was carried out using this core domain, including the addition of random DNA and RNA. Both RaPID selection against full-length and core SIRT7 enriched for peptide sequences (Figure 5C, Supporting Figure S6B). We found that the protein target no longer bound the mRNA displayed peptides through the nucleic acids (Supporting Figure S6C,D). The top peptides from each of the two modified selections were therefore carried forward for synthesis and *in vitro* testing. These top peptides both contained multiple cysteines which introduces the possibility of

multiple macrocycles forming. However, according to previous reports,[36] the smaller of the cycles are kinetically preferred. To ensure that only one cyclic structure is formed, and to avoid potential disulfide bond formation, the cyclic peptides were synthesized using solid-phase peptide synthesis (SPPS) with the C-terminal cysteines mutated to alanine: **IJ4** (Supplementary Figure S6E) and **IJ5** (Figure 5D).

Both peptides **IJ4** and **IJ5** could inhibit that activity of tRNA-activated SIRT7, with IC_{50} = 25 ± 4.2 μM and 0.7 ± 0.38 μM, respectively (Supplementary Figure S6F). Relative to **34**, **IJ4** has similar potency, whereas **IJ5** exhibits an order of magnitude higher potency (Supplementary Figure S6F).

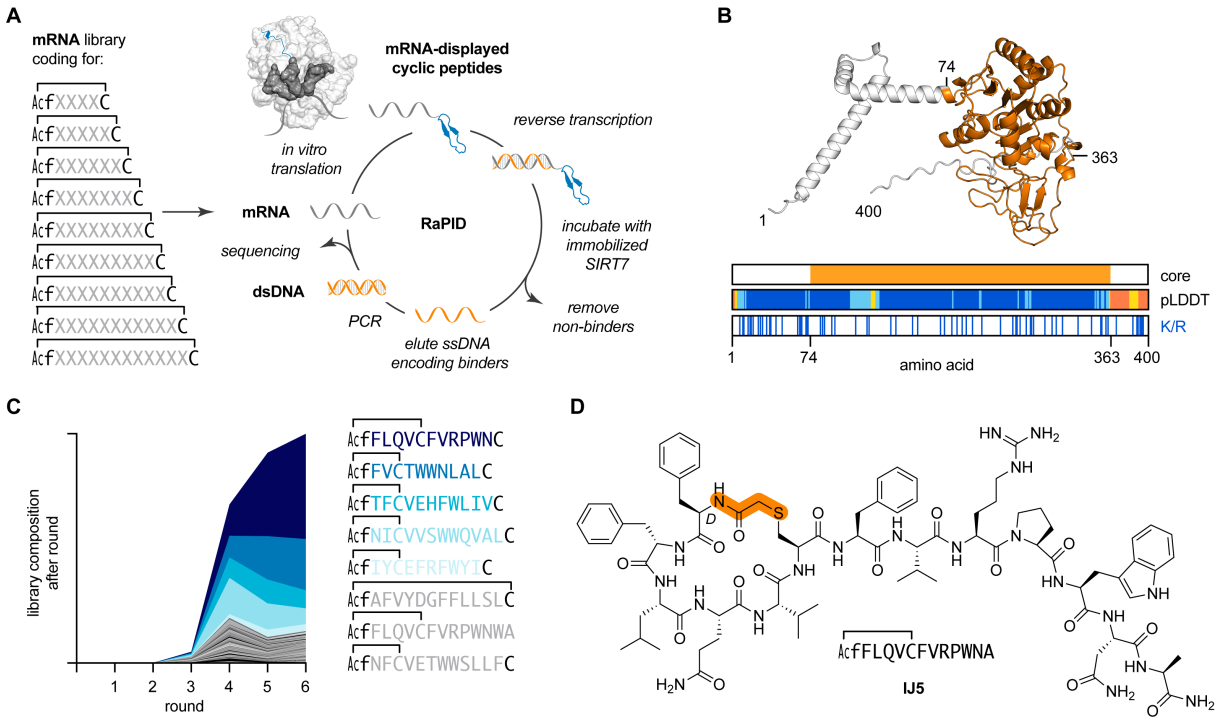

Figure 5. *De novo* cyclic peptides were discovered for SIRT7. (**A**) Overview of RaPID selection, starting from a mRNA library encoding cyclic peptides with 4–12 randomized amino acids, where X can be any of canonical amino acids (apart from methionine). (**B**) Design of construct of just the enzymatic core of SIRT7 (orange), guided by the AlphaFold2 structure prediction (shown), confidence measures (pLDDT), and distribution of lysine and arginine (K/R). (**C**) Sequencing of RaPID selection against the core domain of SIRT7, showing enrichment of peptide sequences. (**D**) Structure of the top cyclic peptide from the core SIRT7 RaPID selection, with a C-terminal cysteine to alanine mutation: **IJ5**. The point of cyclization through internal cysteine (C6) and N-terminal chloroacetyl group to give a thioether functionality is highlighted by orange shading.

Finally, we tested the three most potent tripeptide inhibitors and the cyclic peptide (**IJ5**) against five different recombinant sirtuin isoforms: SIRT1–3, 5, and 6 (catalytically active SIRT4 is not commercially available). Like the parent compound (**3**), we still observed notable inhibition of class I sirtuins for compound **27** (thiourea). Its inverse thioamide analogue **34** also inhibited SIRT1, 2, and 6 to a substantial extent at 10 μM inhibitor concentration, while the inverse amide (**33**) exhibited lower degree of inhibition of SIRT2 deacetylation and only limited inhibition of SIRT3 at 10 μM concentration (Figure 6A). These results therefore corroborate the previous

indication[20b] that the choice of inverse amide-based chemotypes has potential in future efforts to improve the potency and selectivity of inhibitors of SIRT7 further. The most selective compound was **IJ5**, was devoid of inhibition of SIRT2 but inhibited SIRT3 to some extent at 10 μM (Figure 6A). We therefore performed full dose–response experiments with **IJ5** against SIRT7 and SIRT3 (Figure 6B), revealing low micromolar potency of **IJ5** against SIRT7 (K_i = 2.1 μM) and selectivity in favour of the desired target, for the first time.

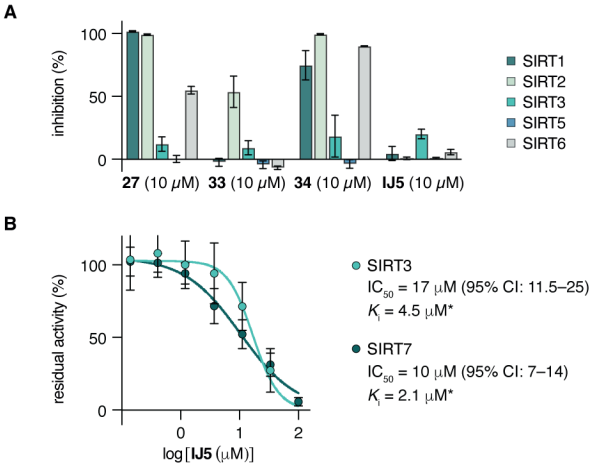

Figure 6. Assessment of the final SIRT7 inhibitor series. (**A**) Assessment of inhibition towards the other sirtuin subtypes using Ac-QPKKac-AMC (SIRT1–3), Ac-LGKsuc-AMC (SIRT5), and Ac-ETDKmyr-AMC (SIRT6) as substrates. (**B**) Dose–response curves, IC_{50} values, and K_i values (*estimated by the Cheng-Prusoff equation) for the inhibition of the deacylation activity of recombinant SIRT7 (500 nM) against the Ac-QPKKdec-AMC (**1b**) substrate (50 μM) in the presence of NAD^+ (500 μM) and nucleosomes or recombinant SIRT3 (300 nM) against NAD^+ (500 μM) and Ac-QPKKmyr-AMC substrate [10 μM; K_M value = 3.6 μM].[28]

Conclusion

In summary, we first expressed catalytically active SIRT7, characterized it biophysically using SAXS, and established conditions for assaying SIRT7 modulators by screening for the activity of our expressed enzyme against a collection of >40 different small fluorophore-conjugated peptides.

Our SAXS data provide experimental insight into the structure of a non-tagged, catalytically functional SIRT7 enzyme for the first time; although, the resolution of SAXS ranges from 50–10 Å.[37] Thus, the SAXS data revealed that SIRT7 is a monomer with low structural flexibility in solution. Further, Coral modeling guided by the SAXS data, and using the AlphaFold2 structure of SIRT7 as starting point, provided a model of the globular structure of SIRT7, which, contrary to the AlphaFold2 structure, presented a C-terminus that does not bind to the Rossman domain. However, AlphaFold2 confidently predicts the full-length SIRT7 to be highly non-globular, including single, solvent-exposed a-helices of the N-terminus projecting at a defined angle from the enzymatic core, and the SAXS data largely support this prediction.

In agreement with previous investigations using longer peptide substrates in an HPLC-based assay format, we found that substrates containing longer acyl modifications to be most efficiently hydrolyzed,[13a, 14] with Kdec-containing substrates being the preferred We also noticed from our screening that peptide sequences

containing a positive charge were preferred over neutral and negatively charged sequences, which is in accordance with demonstrated targets of SIRT7 (*i.e.,* H3K18 and H3K36).[6a, 6f, 38] This also agrees with the previously proposed hypothesis that the negatively charged oligonucleotides enable the formation of a ternary complex (substrate–oligonucleotide–SIRT7),[6f] which was also supported by an observed a Hook effect for both DNA and tRNA as activators. Unlike the behavior of SIRT6, which is known to be activated by fatty acids,[15a, 15d] neither decanoic nor myristic acid activated SIRT7. Reconstituted nucleosomes, on the other hand, activated the catalytic removal of acyl groups substantially more than the tRNA (>4-fold), and whereas Michaelis-Menten parameters could not be determined using tRNA, the addition of nucleosomes allowed for determination of kinetic parameters of the system.

Next, we focused on the development of inhibitors of SIRT7. Only three examples of SIRT7 inhibitors were previously reported, a small molecule and two cyclic peptide analogues.[20] The cyclic peptides also exhibited potent inhibition of SIRT1–3 and 6, with SIRT2 being inhibited 10-fold more potently than SIRT7[20b] and selectivity was not addressed for the small molecule-based inhibitor, leaving ample room for further development of inhibitors. Thus, we performed the first SAR study reported for development of SIRT7 inhibitors, where we iteratively designed and tested 30 tripeptide analogues to optimize the amino acid sequence, the N-terminal functional group, and the ε-*N*-acyllysine mimicking motif. Unfortunately, the most potent compounds [**33** (IC_{50} 44 μM) and **34** (IC_{50} 34 μM)] exhibited more potent inhibition of SIRT2 than SIRT7.

We therefore finally turned to screening of large libraries of random peptides to find *de novo* inhibitors of SIRT7, using the RaPID system, which allows screening of trillions of cyclic peptides. The top hits from selection for binding to either the full-length SIRT7 or the core enzymatic domain were **IJ4** and **IJ5**, respectively. The **IJ5** peptide had a 10-fold higher potency than the best mechanism-based inhibitor (**34**) and is the most potent inhibitor of *in vitro* SIRT7 activity reported to the best of our knowledge. Further, **IJ5** is the first compound to exhibit selectivity for SIRT7 over other sirtuin isoforms, which renders this molecule a promising starting point for the development of more potent and specific inhibitors needed to fully investigate the SIRT7 *in vivo.*

Supporting information

Supporting Information includes figures, tables, experimental methods, compound characterization data, copies of HPLC chromatograms, and copies of NMR spectra for synthesized compounds.

Acknowledgements

We thank Tobias N. Hansen for assistance with SIRT assays. We acknowledge DESY (Hamburg, Germany), a member of the Helmholtz Association HGF, for providing beam time for the SAXS experiments and provision of experimental facilities; the data were collected at PETRA III beamline P12 operated by EMBL Hamburg. Beamtime was allocated for proposal SAXS-734. This project has received funding from the European Research

Council (ERC) under the European Union's Horizon 2020 Research and Innovation Programme (grant agreement number: 725172–*SIRFUNCT*; C.A.O.).

Declaration of interest

The authors declare no competing interests.

References

[1] a) P. Bheda, H. Jing, C. Wolberger, H. Lin, *Annu Rev Biochem* **2016**, *85*, 405-429; b) N. Rajabi, I. Galleano, A. S. Madsen, C. A. Olsen, in *Progress in Molecular Biology and Translational Science, Vol. 154* (Ed.: W. Zheng), Academic Press, **2018**, pp. 25-69.

[2] a) E. Ford, R. Voit, G. Liszt, C. Magin, I. Grummt, L. Guarente, *Genes Dev* **2006**, *20*, 1075-1080; b) S. Kiran, N. Chatterjee, S. Singh, S. C. Kaul, R. Wadhwa, G. Ramakrishna, *Febs J* **2013**, *280*, 3451-3466.

[3] a) H. S. Lee, W. Jung, E. Lee, H. Chang, J. H. Choi, H. G. Kim, A. Kim, B. H. Kim, *J Pathol Transl Med* **2016**, *50*, 337-344; b) M. Fukuda, et al. Yamagata, *Nat Comm* **2018**, *9*, 2833.

[4] X. Bao, Z. Liu, W. Zhang, K. Gladysz, Y. M. E. Fung, G. Tian, Y. Xiong, J. W. H. Wong, K. W. Y. Yuen, X. D. Li, *Mol Cell* **2019**, *76*, 660-675.e669.

[5] L. Li, L. Shi, S. Yang, R. Yan, D. Zhang, J. Yang, L. He, W. Li, X. Yi, L. Sun, J. Liang, Z. Cheng, L. Shi, Y. Shang, W. Yu, *Nat Commun* **2016**, *7*, 12235.

[6] a) M. F. Barber, E. Michishita-Kioi, Y. Xi, L. Tasselli, M. Kioi, Z. Moqtaderi, R. I. Tennen, S. Paredes, N. L. Young, K. Chen, K. Struhl, B. A. Garcia, O. Gozani, W. Li, K. F. Chua, *Nature* **2012**, *487*, 114-118; b) M. F. Karim, T. Yoshizawa, Y. Sato, T. Sawa, K. Tomizawa, T. Akaike, K. Yamagata, *Biochem Biophys Res Commun* **2013**, *441*, 157-163; c) B. N. Vazquez, J. K. Thackray, N. G. Simonet, N. Kane-Goldsmith, P. Martinez-Redondo, T. Nguyen, S. Bunting, A. Vaquero, J. A. Tischfield, L. Serrano, *The EMBO Journal* **2016**, *35*, 1488-1503; d) K. Tanabe, J. Liu, D. Kato, H. Kurumizaka, K. Yamatsugu, M. Kanai, S. A. Kawashima, *Sci Rep* **2018**, *8*, 2656; e) D. Wu, Y. Li, K. S. Zhu, H. Wang, W.-G. Zhu, *Front Endocrinol* **2018**, *9*; f) W. W. Wang, M. Angulo-Ibanez, J. Lyu, Y. Kurra, Z. Tong, B. Wu, L. Zhang, V. Sharma, J. Zhou, H. Lin, Y. Q. Gao, W. Li, K. F. Chua, W. R. Liu, *J Am Chem Soc* **2019**, *141*, 2462-2473.

[7] a) Y. C. Tsai, T. M. Greco, A. Boonmee, Y. Miteva, I. M. Cristea, *Mol Cell Proteomics* **2012**, *11*, 60-76; b) S. Chen, J. Seiler, M. Santiago-Reichelt, K. Felbel, I. Grummt, R. Voit, *Mol Cell* **2013**, *52*, 303-313; c) S. Chen, M. F. Blank, A. Iyer, B. Huang, L. Wang, I. Grummt, R. Voit, *Nature Communications* **2016**, *7*, 10734; d) A. Ianni, S. Hoelper, M. Krueger, T. Braun, E. Bober, *Biochem Biophys Res Commun* **2017**, *492*, 434-440; e) A. Iyer-Bierhoff, N. Krogh, P. Tessarz, T. Ruppert, H. Nielsen, I. Grummt, *Cell Rep* **2018**, *25*, 2946-2954.e) 2945; fS. Paredes, M. Angulo-Ibanez, L. Tasselli, S. M. Carlson, W. Zheng, T. M. Li, K. F. Chua, *J Biol Chem* **2018**, *293*, 11242-11250.

[8] J. Shin, M. He, Y. Liu, S. Paredes, L. Villanova, K. Brown, X. Qiu, N. Nabavi, M. Mohrin, K. Wojnoonski, P. Li, H. L. Cheng, A. J. Murphy, D. M. Valenzuela, H. Luo, P. Kapahi, R. Krauss, R. Mostoslavsky, G. D. Yancopoulos, F. W. Alt, K. F. Chua, D. Chen, *Cell Rep* **2013**, *5*, 654-665.

[9] D. Ryu, Y. S. Jo, G. Lo Sasso, S. Stein, H. Zhang, A. Perino, J. U. Lee, M. Zeviani, R. Romand, M. O. Hottiger, K. Schoonjans, J. Auwerx, *Cell Metab* **2014**, *20*, 856-869.

[10] a) T. Yoshizawa, M. F. Karim, Y. Sato, T. Senokuchi, K. Miyata, T. Fukuda, C. Go, M. Tasaki, K. Uchimura, T. Kadomatsu, Z. Tian, C. Smolka, T. Sawa, M. Takeya, K. Tomizawa, Y. Ando, E. Araki,

T. Akaike, T. Braun, Y. Oike, E. Bober, K. Yamagata, *Cell Metab* **2014**, *19*, 712-721; b) H. Hu, W. Zhu, J. Qin, M. Chen, L. Gong, L. Li, X. Liu, Y. Tao, H. Yin, H. Zhou, L. Zhou, D. Ye, Q. Ye, D. Gao, *Hepatology* **2017**, *65*, 515-528.

[11] S. Kiran, T. Anwar, M. Kiran, G. Ramakrishna, *Cellular Signalling* **2015**, *27*, 673-682.

[12] a) M. Ding, C.-Y. Jiang, Y. Zhang, J. Zhao, B.-M. Han, S.-J. Xia, *Journal of Experimental & Clin Cancer Res* **2020**, *39*, 28; b) J. K. Kim, J. H. Noh, K. H. Jung, J. W. Eun, H. J. Bae, M. G. Kim, Y. G. Chang, Q. Shen, W. S. Park, J. Y. Lee, J. Borlak, S. W. Nam, *Hepatology* **2013**, *57*, 1055-1067; c) H. Yu, W. Ye, J. Wu, X. Meng, R. Y. Liu, X. Ying, Y. Zhou, H. Wang, C. Pan, W. Huang, *Clin Cancer Res* **2014**, *20*, 3434-3445.

[13] a) Z. Tong, M. Wang, Y. Wang, D. D. Kim, J. K. Grenier, J. Cao, S. Sadhukhan, Q. Hao, H. Lin, *ACS Chem Biol* **2017**, *12*, 300-310; b) V. I. Kuznetsov, W. H. Liu, M. A. Klein, J. M. Denu, *ACS Chem Biol* **2022**, *17*, 2248-2261.

[14] Z. Tong, Y. Wang, X. Zhang, D. D. Kim, S. Sadhukhan, Q. Hao, H. Lin, *ACS Chem Biol* **2016**, *11*, 742-747.

[15] a) J. L. Feldman, J. Baeza, J. M. Denu, *J Biol Chem* **2013**, *288*, 31350-31356; b) W. You, D. Rotili, T. M. Li, C. Kambach, M. Meleshin, M. Schutkowski, K. F. Chua, A. Mai, C. Steegborn, *Angew Chem Int Ed Engl* **2017**, *56*, 1007-1011; c) Z. Huang, J. Zhao, W. Deng, Y. Chen, J. Shang, K. Song, L. Zhang, C. Wang, S. Lu, X. Yang, B. He, J. Min, H. Hu, M. Tan, J. Xu, Q. Zhang, J. Zhong, X. Sun, Z. Mao, H. Lin, M. Xiao, Y. E. Chin, H. Jiang, Y. Xu, G. Chen, J. Zhang, *Nat Chem Biol* **2018**, *14*, 1118-1126; d) M. A. Klein, C. Liu, V. I. Kuznetsov, J. B. Feltenberger, W. Tang, J. M. Denu, *J Biol Chem* **2020**, *295*, 1385-1399.

[16] a) R. Gil, S. Barth, Y. Kanfi, H. Y. Cohen, *Nucleic Acids Res* **2013**, *41*, 8537-8545; b) Z. A. Wang, J. W. Markert, S. D. Whedon, M. Yapa Abeywardana, K. Lee, H. Jiang, C. Suarez, H. Lin, L. Farnung, P. A. Cole, *J Am Chem Soc* **2023**, *145*, 6811-6822; c) U. S. Chio, O. Rechiche, A. R. Bryll, J. Zhu, E. M. Leith, J. L. Feldman, C. L. Peterson, S. Tan, J. P. Armache, *Sci Adv* **2023**, *9*, eadf7586.

[17] W. H. Liu, J. Zheng, J. L. Feldman, M. A. Klein, V. I. Kuznetsov, C. L. Peterson, P. R. Griffin, J. M. Denu, *Nat Commun* **2020**, *11*, 5244.

[18] a) M. Hałasa, D. Bartuzi, D. Cieślak, A. A. Kaczor, P. Miziak, A. Stepulak, D. Matosiuk, *J Biomol Struct Dyn* **2020**, *38*, 1283-1291; b) J. Jumper, et al, *Nature* **2021**, *596*, 583-589.

[19] A. Priyanka, V. Solanki, R. Parkesh, K. G. Thakur, *Proteins* **2016**, *84*, 1558-1563.

[20] aJ. H. Kim, D. Kim, S. J. Cho, K. Y. Jung, J. H. Kim, J. M. Lee, H. J. Jung, K. R. Kim, *Biochem Biophys Res Commun* **2019**, *508*, 451-457; bS. Li, B. Wu, W. Zheng, *Bioorg Med Chem Lett* **2019**, *29*, 461-465.

[21] a) K. Tunyasuvunakool, et al. Hassabis, *Nature* **2021**, *596*, 590-596; b) T. Lazar, et al, *Nucleic Acids Res* **2021**, *49*, D404-D411.

[22] P. W. Pan, J. L. Feldman, M. K. Devries, A. Dong, A. M. Edwards, J. M. Denu, *J Biol Chem* **2011**, *286*, 14575-14587.

[23] W. You, C. Steegborn, *Nat Chem Biol* **2021**, *17*, 519-521.

[24] Z. Huang, et al. Zhang, *Nat Chem Biol* **2021**, *17*, 522-523.

[25] a) A. S. Madsen, C. A. Olsen, *J Med Chem* **2012**, *55*, 5582-5590; b) A. S. Madsen, C. Andersen, M. Daoud, K. A. Anderson, J. S. Laursen, S. Chakladar, F. K. Huynh, A. R. Colaço, D. S. Backos, P. Fristrup, M. D. Hirschey, C. A. Olsen, *J Biol Chem* **2016**, *291*, 7128-7141; c) I. Galleano, M. Schiedel, M. Jung, A. S. Madsen, C. A. Olsen, *J Med Chem* **2016**, *59*, 1021-1031; d) C. Moreno-Yruela, I.

Galleano, A. S. Madsen, C. A. Olsen, *Cell Chem Biol* **2018**, *25*, 849-856.e848; e) S. V. Olesen, N. Rajabi, B. Svensson, C. A. Olsen, A. S. Madsen, *Biochemistry* **2018**, *57*, 3903-3915; f) N. Rajabi, A. L. Nielsen, C. A. Olsen, *ACS Med. Chem Lett* **2020**, *11*, 1886-1892; g) C. Moreno-Yruela, D. Zhang, W. Wei, M. Bæk, W. Liu, J. Gao, D. Danková, A. L. Nielsen, J. E. Bolding, L. Yang, S. T. Jameson, J. Wong, C. A. Olsen, Y. Zhao, *Sci Adv* **2022**, *8*, eabi6696.

[26] a) K. Hoffmann, G. Brosch, P. Loidl, M. Jung, *Nucleic Acids Res* **1999**, *27*, 2057-2058; bD. Wegener, F. Wirsching, D. Riester, A. Schwienhorst, *Chem Biol* **2003**, *10*, 61-68; c) B. Heltweg, F. Dequiedt, B. L. Marshall, C. Brauch, M. Yoshida, N. Nishino, E. Verdin, M. Jung, *J Med Chem* **2004**, *47*, 5235-5243.

[27] M. F. Blank, I. Grummt, *Transcription* **2017**, *8*, 67-74.

[28] Y.-L. Chiang, H. Lin, *Org Biomol Chem* **2016**, *14*, 2186-2190.

[29] a) N. Rajabi, M. Auth, K. R. Troelsen, M. Pannek, D. P. Bhatt, M. Fontenas, M. D. Hirschey, C. Steegborn, A. S. Madsen, C. A. Olsen, *Angew Chem Int Ed Engl* **2017**, *56*, 14836-14841; b) A. L. Nielsen, N. Rajabi, N. Kudo, K. Lundø, C. Moreno-Yruela, M. Bæk, M. Fontenas, A. Lucidi, A. S. Madsen, M. Yoshida, C. A. Olsen, *RSC Chem Biol* **2021**, *2*, 612-626; c) K. S. Troelsen, M. Bæk, A. L. Nielsen, A. S. Madsen, N. Rajabi, C. A. Olsen, *RSC Chem Biol* **2021**, *2*, 627-635.

[30] J. L. Avalos, J. D. Boeke, C. Wolberger, *Mol Cell* **2004**, *13*, 639-648.

[31] A. D. Napper, J. Hixon, T. McDonagh, K. Keavey, J.-F. Pons, J. Barker, W. T. Yau, P. Amouzegh, A. Flegg, E. Hamelin, R. J. Thomas, M. Kates, S. Jones, M. A. Navia, J. O. Saunders, P. S. DiStefano, R. Curtis, *Journal of medicinal chemistry* **2005**, *48*, 8045-8054.

[32] H. Jing, J. Hu, B. He, Y. L. Negrón Abril, J. Stupinski, K. Weiser, M. Carbonaro, Y. L. Chiang, T. Southard, P. Giannakakou, R. S. Weiss, H. Lin, *Cancer Cell* **2016**, *29*, 297-310.

[33] J. Morimoto, Y. Hayashi, H. Suga, *Angew Chem Int Ed Engl* **2012**, *51*, 3423-3427.

[34] Y. Goto, H. Suga, *Acc Chem Res* **2021**, *54*, 3604-3617.

[35] M. F. Blank, S. Chen, F. Poetz, M. Schnolzer, R. Voit, I. Grummt, *Nucleic Acids Res* **2017**, *45*, 2675-2686.

[36] K. Iwasaki, Y. Goto, T. Katoh, H. Suga, *Org Biomol Chem* **2012**, *10*, 5783-5786.

[37] C. D. Putnam, M. Hammel, G. L. Hura, J. A. Tainer, *Q Rev Biophys* **2007**, *40*, 191-285.

[38] S. Malik, L. Villanova, S. Tanaka, M. Aonuma, N. Roy, E. Berber, J. R. Pollack, E. Michishita-Kioi, K. F. Chua, *Sci Rep* **2015**, *5*, 9841.

TOC Graphic (11 × 2.5 cm)

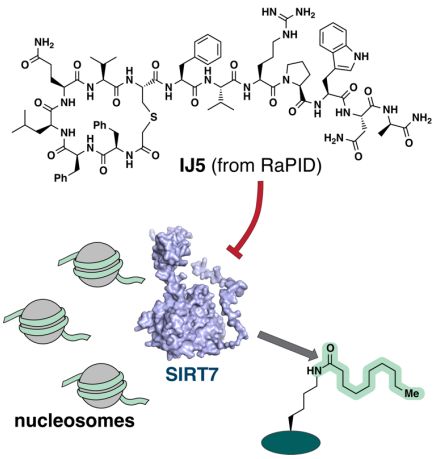

TOC text (max 450 characters)

Broad screening of the substrate specificity of SIRT7 revealed a strong preference for the cleavage of long chain acyl lysine modifications as well as amino acid sequence preferences. Further, the activity was substantially increased in the presence of oligonucleotides or nucleosome particles. Finally, mRNA display selection delivered a cyclopeptide with potency in the low micromolar range.